Chinese Journal of Chemical Engineering 87 (2025) 252–261

Contents lists available at ScienceDirect

Chinese Journal of Chemical Engineering

journal homepage: www.elsevier.com/locate/CJChE

Full Length Article

High-performance 19-channel monolithic CHA zeolite membranes for vapor-permeation dehydration of acetic acid

Hong Xiao , Shilei Yu , Yuhan Yan , Junjing Zhou , Rongfei Zhou *, Weihong Xing

State Key Laboratory of Materials-Oriented Chemical Engineering, College of Chemical Engineering, Nanjing Tech University, Nanjing 210009, China

ARTICLE INFO

Article history:
Received 11 March 2025
Received in revised form
22 April 2025
Accepted 24 April 2025
Available online 1 July 2025

Keywords:
Zeolite membrane
Monolithic
Chabazite
Acetic acid
Vapor permeation

ABSTRACT

Membrane-based vapor permeation (VP) is regarded as a highly efficient technology, featuring low energy consumption and free salt fouling. In this study, we have demonstrated upscaling chabazite (CHA) zeolite membranes on the 19-channel α-Al_2O_3 monolithic supports synthesized from high-silica gel (SiO_2/Al_2O_3 ratio of 200) for the dehydration of acetic acid by VP. The monolithic membrane presents higher surface-to-volume ratio and a-tenfold greater mechanical strength compared to tubular ones. The micromorphology and crystallinity of the monolithic CHA zeolite membranes were characterized by scanning electron micrographs and X-ray diffraction analysis. The single-gas permeation test and the effects of temperature, feed water content and feed flow rate on the VP separation performance of monolithic CHA zeolite membrane for dehydration of acetic acid were investigated. Moreover, the stability test of monolithic CHA zeolite membranes was carried out. The 19-channel monolithic membrane achieved a comparable separation performance (water flux of 0.63 kg $m^{-2}\cdot h^{-1}$ and selectivity of 369 at 393 K) with the reported small-area zeolite membranes in water/acetic acid mixtures. It is demonstrated that the monolithic CHA zeolite membranes could be transformative candidates for industrial dehydration of acetic acid under harsh environments.

1. Introduction

Acetic acid (AcOH) has emerged as a globally significant chemical, serving a critical role in food preservation and industrial applications ranging from pharmaceuticals to polymer synthesis [1–3]. Methanol carbonylation is one of industrial processes for AcOH synthesis, where water as the process medium inevitably infiltrates the final product [4]. On the other hand, AcOH should be purified from water/AcOH mixtures by dehydration for reuse as a solvent. Efficient recovery of AcOH from aqueous mixtures presents substantially technical challenges, primarily due to the near-identical boiling points of water (373 K) and AcOH (391 K), and interaction force between two molecules. Conventional distillation for separation of the mixtures is energy-intensive and economically prohibitive [5,6]. Moreover, the strong corrosion of AcOH during the distillation separation results in high costs for equipment such as distillation towers for anti-corrosion. Recent advancements in membrane-based separation technologies, particularly pervaporation (PV) and vapor permeation (VP), have demonstrated exceptional potential for the dehydration of organic solutions [7]. The two processes offer distinct advantages over distillation through enhanced energy efficiency and operational flexibility [8]. The critical limitation for PV is that the deposition of salts formed from the reused processes on membrane surfaces leads to performance degradation of the membrane. The VP process could effectively minimize the membrane fouling from salt accumulation because the high boiling salt does not exist in the vapor.

Zeolite membranes have been widely used in the dehydration of water/organic mixtures, such as NaA [9–11], T-type [12], MOR [13,14], and MFI [15–18]. It is well established that NaA zeolite membranes with a silicon-to-aluminum-ratio (SAR) of 1.0 have achieved great success in the dehydration of ethanol aqueous mixtures, but they cannot survive in acidic solutions at test temperatures. The aluminum (Al) of Al-rich NaA zeolite framework is easily leached by the attack of H^+ cation in strongly acidic solution [19]. Chabazite (CHA) zeolite membranes have attracted charming attention due to their uniform 8-membered-ring pore structure, three-dimensional channel systems and tunable SAR (2-∞). Jiang *et al.* [20] demonstrated that CHA zeolite membranes prepared on hollow fiber support (4.5 cm^2) displayed increased hydrothermal

* Corresponding author.
E-mail address: rf-zhou@njtech.edu.cn (R. Zhou).

https://doi.org/10.1016/j.cjche.2025.04.021

and acidic stabilities. Hasegawa *et al.* [21] synthesized CHA zeolite membranes (SAR = 3.2) on the α-Al_2O_3 tubular support (1.9 cm^2) displayed high PV separation performance (water flux of 4.14 $kg \cdot m^{-2} \cdot h^{-1}$, separation factor of 39500) in 90% (mass) ethanol aqueous solution at 348 K; These membranes were stable in acidic solution (pH ~ 2) for 10 h. Qiu *et al.* [22] investigated the long-term stability (over 35 h) for AcOH dehydration of CHA zeolite membranes (SAR = 3.6) prepared on hollow fiber support (5.8 cm^2) using cheap choline chloride as templates. Imasaka *et al.* [23] reported the preparation of high-silica CHA zeolite membranes on a α-Al_2O_3 support tube (30 cm^2), which achieved a water flux of 2.1 $kg \cdot m^{-2} \cdot h^{-1}$ and water/AcOH separation factor of 401 by PV in a 70% (mass) AcOH aqueous solution at 348 K.

Most of the reported zeolite membranes are prepared on tubular supports. They suffer two challenges: 1) the membrane area and surface-to-volume ratio of a single membrane element are limited, bringing the low packing density of the final membrane module, the low packing efficiency, and the requirement of a large amount of sealing elements; 2) to deal with the corrosive separation system such as AcOH aqueous solution, the corrosive feed directly contacts the metal module when outside tubular membrane is used, resulting in the high costs for membrane modules made from special steels. On the other hand, the reports for VP separation of water/AcOH mixtures are scarce because of the lack of highly acid-stable membranes. Monolithic and inside membrane provides the superior advantages to overcome the above challenges. The surface area and surface-to-volume ratio of monolithic membrane element are times higher than those of tubular ones; in addition, the mechanical strength of the former is one order of magnitude higher than that of the latter [24]. Most importantly, zeolite layers of monolithic membranes are grown on the inside surface of the channels of monolithic support, which allows the corrosive and hot feed goes through inside acid-stable zeolite membranes rather than the shell side to reduce the cost of membrane modules. In our previous study [25], we prepared low-silica CHA membranes (SAR = 3.5) on monolithic supports, which showed excellent separation performance in a mass ratio of 10/90 water/ethanol mixtures. Nevertheless, this membrane was unstable for the dehydration of AcOH.

In this work, we have evaluated the large-area 19-channel monolithic high-silica CHA zeolite membranes for the dehydration of AcOH by VP. It should be noted that the membrane area of 19-channel monolithic CHA zeolite membranes was an order of magnitude larger than that of most membranes in the literatures [26–29]. We comprehensively investigated the single gas permeation and the effects of temperature, feed water content and feed flow rate on the VP performance of 19-channel monolithic CHA zeolite membranes. Permeance and selectivity, reflected the inherent separation performance of the membranes together with flux and separation factor, were provided in this study. The monolithic CHA zeolite membranes exhibited the water flux of 0.63 $kg \cdot m^{-2} \cdot h^{-1}$, water permeance of 8.56×10^{-8} $mol \cdot m^{-2} \cdot s^{-1} \cdot Pa^{-1}$ and selectivity of 369, which was comparable to that of the reported small-area membranes. Additionally, the stability of monolithic high-silica CHA zeolite membranes for dehydration of AcOH under high-temperature and corrosive environments was further explored.

2. Experimental

2.1. Synthesis of high-silica CHA zeolite seeds

High-silica CHA zeolite seeds (~200 nm) were synthesized *via* a hydrothermal reaction adapted from our prior methodology [30]. Reagent-grade chemicals were employed without additional purification. A precursor gel was prepared by dissolving 3.52 g of sodium hydroxide (NaOH, 96% (mass), Sinopharm, China) and 142.84 g of *N,N,N*-trimethtyl-1-adamantammonium hydroxide (TMAdaOH, 25% (mass) in water, homemade) in 189.35 g of deionized water under ambient stirring conditions for 1 h; And 0.83 g of aluminum hydroxide ($Al(OH)_3$, 99% (mass), Wako Pure Chemical, Japan) was subsequently introduced into the alkaline medium solutions under vigorous agitation for 2 h. Finally, 63.45 g of colloidal silica (LUDOX TM-40, 40% (mass) aqueous suspension, Sigma-Aldrich, China) was added in to the gel for aging 12 h at ambient environment. The molar ratio in the synthesized gel was 1.0 SiO_2: 0.2 NaOH: 0.025 $Al(OH)_3$: 0.4 TMAdaOH: 44 H_2O. The 400 g synthesis gel was transferred to an autoclave lined with polytetrafluoroethylene (PTFE) and hydrothermal synthesis was carried out at 433 K for 96 h. After synthesis, the solution was centrifuged at 8000 $r \cdot min^{-1}$ for 10 min, and this washing procedure was repeated three times until neutral pH was achieved, high-silica CHA zeolite crystals were recovered and dried overnight at 333 K. The samples were calcined in air to remove organic structural directing agent (OSDA) at 823 K for 10 h, with heating and cooling rates of 10 $K \cdot min^{-1}$.

2.2. Synthesis of 19-channel monolithic CHA zeolite membranes

Monolithic CHA zeolite membranes were prepared in a high-silica gel with SiO_2/Al_2O_3 ratio of 200 on 19-channel α-Al_2O_3 monolithic supports (OD of 30 mm, ID of 4 mm, average pore size of 200 nm and Jiangsu Membrane Park Co., Ltd. in China) by secondary growth. To fit the length of the membrane module, the support was sectioned into segments with a length of 6.5 cm. The above seed crystals (0.5 g) were dispersed in ethanol (1000 g) *via* continuous ultrasonication (40 kHz) for 6 h to obtain a uniform seed suspension with mass concentration of 0.05%. Vacuum seeding procedure enabled uniform anchoring of the seed layer onto the monolithic support, which was similar to our previous method [31]. The precursor gel for secondary growth of membrane was formulated by mixing NaOH, TMAdaOH, $Al(OH)_3$ and colloidal silica. The preparation procedure and chemical sources were similar to the above ones for seed preparation, but the molar ratio of the membrane gel was 1.0 SiO_2: 0.2 NaOH: 0.01 $Al(OH)_3$: 0.3 TMAdaOH: 44 H_2O. The 300 g precursor gel and seeded monolithic support were placed in the autoclave under hydrothermal crystallization at 453 K for 96 h. Post-synthesis, membranes were calcined under O_2 flow with flow rate of 400 $ml \cdot min^{-1}$ at 673 K for 6 h to remove the OSDAs with heating and cooling rates of 1 $K \cdot min^{-1}$.

2.3. Characterization

The morphology of surface and cross-section for monolithic membranes with various channels was analyzed using a field-emission scanning electron microscope (FE-SEM, Hitachi S-4800, Japan) at voltages ranging from 5 to 10 kV. Prior to testing, the samples were dried in a preheated oven to remove moisture and then coated with a thin layer of Au under vacuum. Additionally, the crystalline layers on the α-Al_2O_3 supports were analyzed by X-ray diffraction (XRD) using a MiniFlex600 (Rigaku, Japan) device, featuring a Cu target and X-ray tube with a 600 W power output. Membrane samples were sectioned into 1 cm^2 planar geometries and analyzed across a 2θ range of 5°–45° at a scanning rate of 1 $(°) \cdot min^{-1}$.

2.4. Single gas permeation and VP measurements

The experimental setup used to evaluate the single gas permeability of the monolithic CHA zeolite membrane was similar to our previous methodology [32], with single gas testing of H_2, N_2,

CO_2, CH_4, and SF_6 by dead-end mode at 298 K and a pressure drop of 0.2 MPa.

The VP test for water/AcOH mixtures was conducted on a homemade device as illustrated in Fig. 1. The monolithic CHA zeolite membrane was sealed in the membrane module using acid-resistant and high-temperature-resistant perfluoro *O*-rings (Fluor elastomer material, Wuxi Aktewe New Material Co., Ltd, China, temperature resistance: 273–503 K). A metering pump was used for transferring the water/AcOH mixture from the feed tank to membrane module passing through the hot oil bath for vaporization. The temperature of the system was maintained in the temperature range from 393 to 413 K for VP testing by precisely regulating the temperature of the hot oil bath. It should be noted that all the conveying pipelines were accompanied by heating tape to minimize the heat loss of the system. At the permeate side, the absolute pressure in the permeate was approximately 100 Pa by a vacuum pump. Moreover, a cold trap in a liquid–nitrogen (77 K) bath was used for condensing the permeated vapor. The vapor at the retentate side was cooled to ambient temperature through a condenser and then reintroduced into the feed tank for recycling. The molar composition of samples at the feed, permeate and retentate sides was analyzed using a meteorological chromatograph (GC-2014, Shimadzu, Japan).

The flux (J_i, $kg \cdot m^{-2} \cdot h^{-1}$) was calculated by the mass (m_i, kg) of component i dividing by the effective area (A, m^2) of the membrane and test time (t, h) as shown in the following equation:

$$J_i = m_i / A\, t \tag{1}$$

The separation factor (SF) is calculated as follows:

$$\mathrm{SF} = \frac{y_i / y_j}{x_i / x_j} \tag{2}$$

where y and x respectively represent component concentrations in permeate and feed side, with subscripts i and j denoting constituents of water and AcOH.

Permeance (P_i, $mol \cdot m^{-2} \cdot s^{-1} \cdot Pa^{-1}$) as a pressure-drop-normalized flux is calculated by the following equation:

$$P_i = J_i / \Delta p_i \tag{3}$$

where $\Delta p_{i,\mathrm{VP}}$ (Pa) for VP is calculated as follows:

$$\Delta p_{i,\mathrm{VP}} = p_{\mathrm{fi}} - p_{\mathrm{pi}} = x_i p_{\mathrm{f}} - y_i p_{\mathrm{p}} \tag{4}$$

where p_{fi} (Pa) and x_i denote the partial pressure and mole fraction of component i in the feed, and p_{pi} (Pa) and y_i denote the partial pressure and mole fraction of component i in the permeate.

The selectivity is given by the following equation:

$$\alpha_{ij} = P_i \Big/ P_j \tag{5}$$

The Wilson equation is utilized to calculate the activity coefficient (γ_i) for component i:

$$\ln \gamma_i = -\ln\left(x_i + \Lambda_{ij} x_j\right) + x_j \left(\frac{\Lambda_{ij}}{x_i + \Lambda_{ij} x_j} - \frac{\Lambda_{ji}}{x_j + \Lambda_{ji} x_i} \right) \tag{6}$$

$$\Lambda_{ij} = \frac{V_j'}{V_i'} \exp\left(-\frac{\lambda_{ij} - \lambda_{ii}}{RT} \right) \tag{7}$$

where the mole fractions of components i and j are denoted as V_i' and V_j', respectively, while the binary energy parameters (λ_{ij}, λ_{ii}) for the Wilson model applied to the water/AcOH mixture are obtained from reported literature [33]. The variation of activity coefficient (γ_i) with feed concentration and temperature is shown in Fig. 2.

The activation energy (E_a) of the permeation is calculated from the Arrhenius equation:

$$K = A \exp(E_a / RT) \tag{8}$$

The Reynolds number (Re) under VP test conditions is given by the following:

$$Re = \frac{\rho v d}{\mu} \tag{9}$$

where ρ is the fluid density ($kg \cdot m^{-3}$), v is the fluid velocity ($m \cdot s^{-1}$), d is the equivalent diameter (mm) and μ is the fluid viscosity (Pa·s).

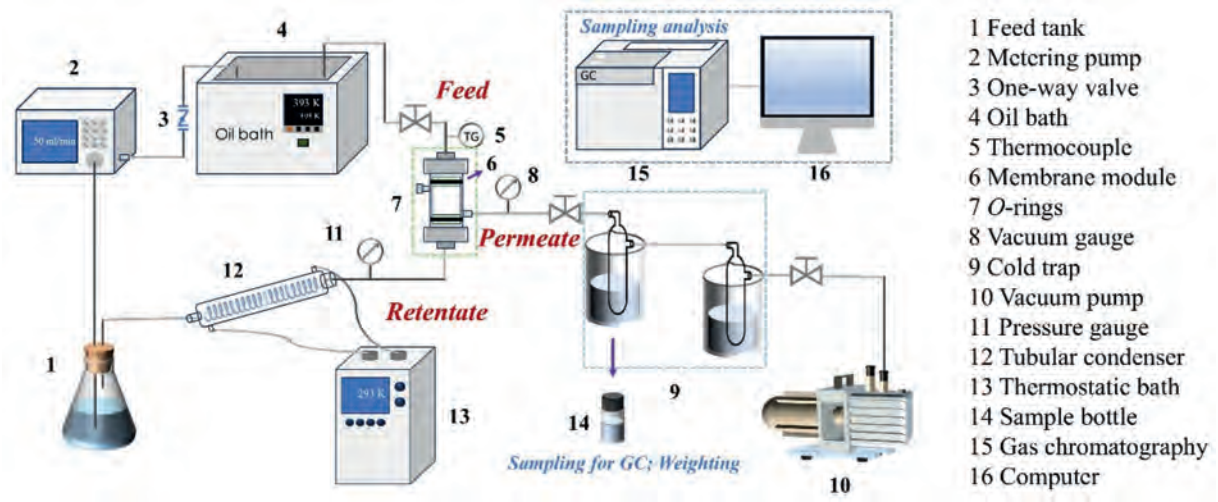

Fig. 1. Schematic diagram of the home-made VP test device.

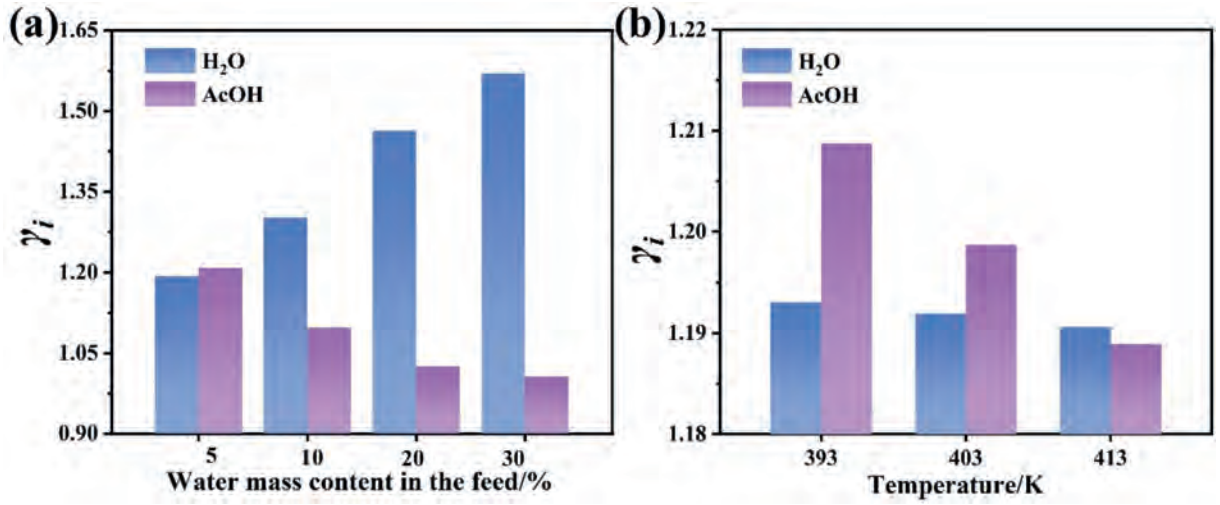

Fig. 2. Activity coefficients as a function of (a) water mass content in the feed, and (b) temperature.

3. Results and Discussion

3.1. Characterization of monolithic CHA zeolite membranes

Fig. 3 shows SEM images of 19-channel monolithic CHA zeolite membranes on channels from the exterior to interior ones (the positions of the detected channel of 19-channel monolith are shown in the inserted figures). The surface of three typical channels were completely covered by a well-intergrown CHA zeolite layer with a similar cubic morphology, exhibiting no obvious defects in the membrane and uniform morphology observed from their surface SEM images in Fig. 3(a)–(c). The thickness of the membrane of the three typical channels was approximately 4.2–4.5 μm, indicating that the growth of membrane on each channel of monolith is uniform (Fig. 3(d)–(f)). Fig. 4 shows the XRD patterns of typical channels of the monolithic CHA zeolite membrane. The diffraction peaks of the membranes grown on the channels from the exterior to interior ones were similar and consisted of typical ones of standard CHA zeolite and alumina support, demonstrating that CHA zeolite membranes are uniform and pure CHA zeolite phase.

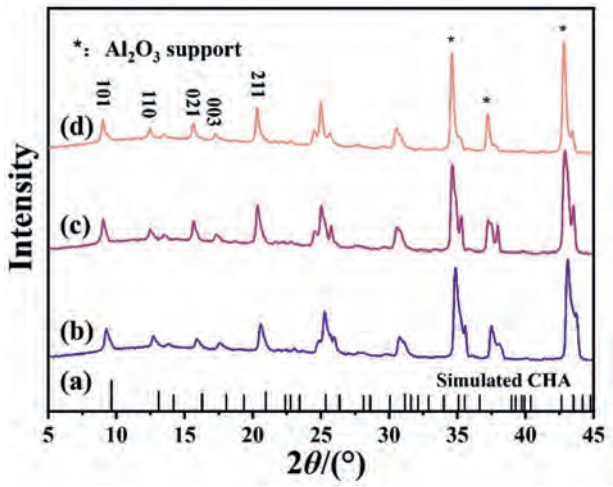

Fig. 4. XRD patterns of (a) simulated CHA framework and CHA zeolite membranes grown on the typical (b) exterior channel, (c) middle channel and (d) interior channel of the monolithic support.

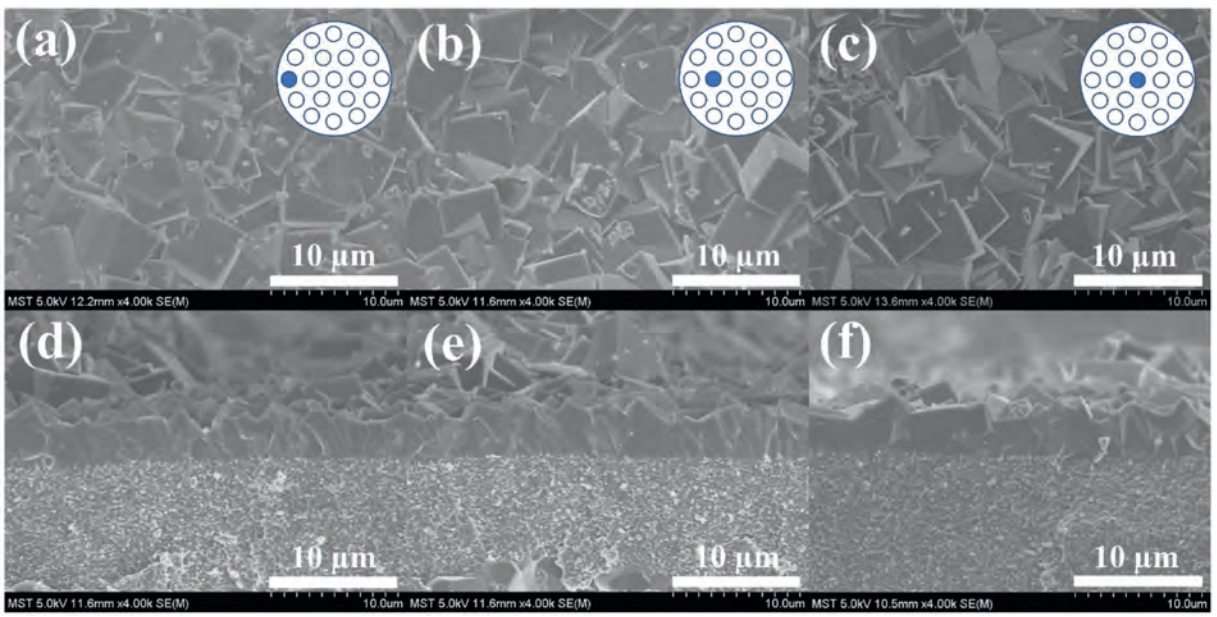

Fig. 3. SEM images of the surface and cross-section of the CHA zeolite membranes grown on the typical (a, d) exterior, (b, e) middle, and (c, f) interior channels of the 19-channel monolithic support. Blue dots in the right upper insert figures represent the sampling channel for SEM detection.

3.2. Single-gas permeation testing

Fig. 5 exhibits the single-gas permeation of CO_2, H_2, N_2, CH_4, and SF_6 through monolithic CHA zeolite membranes at 0.2 MPa and 298 K. For investigating the preparation reproducibility of the monolithic membranes, the single-gas permeation of three membranes prepared under the identical conditions (termed as M1, M2 and M3) were measured, respectively. The permeance of CO_2, H_2, N_2, CH_4, and SF_6 exhibited an inverse correlation with molecular kinetic diameter apart from CO_2. The high CO_2 permeance of membrane M1 was up to 1.36×10^{-7} mol·m^{-2}·s^{-1}·Pa^{-1}, which was attributed to the preferential adsorption of CO_2 on the CHA zeolite [34]. The average ideal selectivities of CO_2/CH_4 and H_2/SF_6 for the three monolithic membranes were 89 ± 17 and 200 ± 20, respectively. It was demonstrated that the monolithic CHA zeolite membranes were uniform with few defects. Meanwhile, the low relative standard deviations of three monolithic membrane for CO_2/CH_4 and H_2/SF_6 were 18.9% and 9.7%, suggesting the high reproducibility of 19-channel monolithic CHA zeolite membranes.

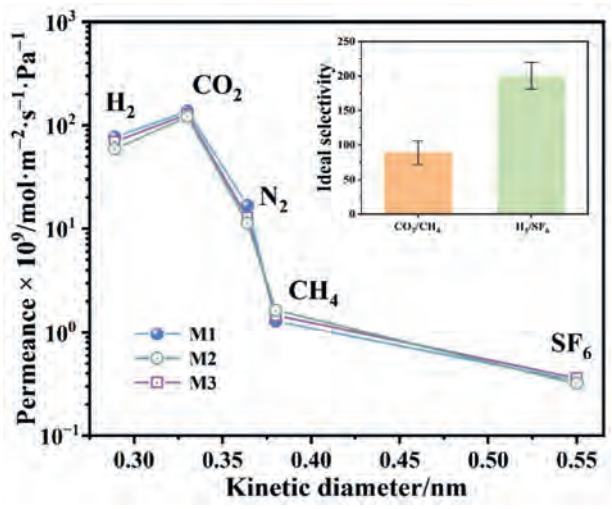

Fig. 5. Permeance of different gases through three 19-channel monolithic CHA zeolite membranes (M1, M2 and M3) prepared under identical conditions at 298 K and 0.2 MPa pressure drop.

3.3. Effect of temperature on VP for monolithic CHA zeolite membranes

Fig. 6 represents the variation of dehydration performance through the monolithic membrane M1 in a mass ratio of 30/70 water/AcOH mixture with temperature. As shown in Fig. 6(a), the water flux and water mass content in the permeate increased from 0.49 to 0.58 kg·m^{-2}·h^{-1} and from 98.99% to 99.39%, respectively, when the test temperature increased from 393 to 413 K. The water permeance decreased by 33%, while AcOH permeance decreased by 60%, leading to an increase of selectivity from 228 to 383 (Fig. 6 (b)). From observation of Fig. 6(c), water flux exhibited strong pressure dependence, whereas the slight decrease of AcOH flux was originated from amplified competitive water adsorption on aluminate-containing CHA zeolite along with the increasing temperature, which was consistent with that in our previous study [35]. Variations of permeance through CHA zeolite membranes

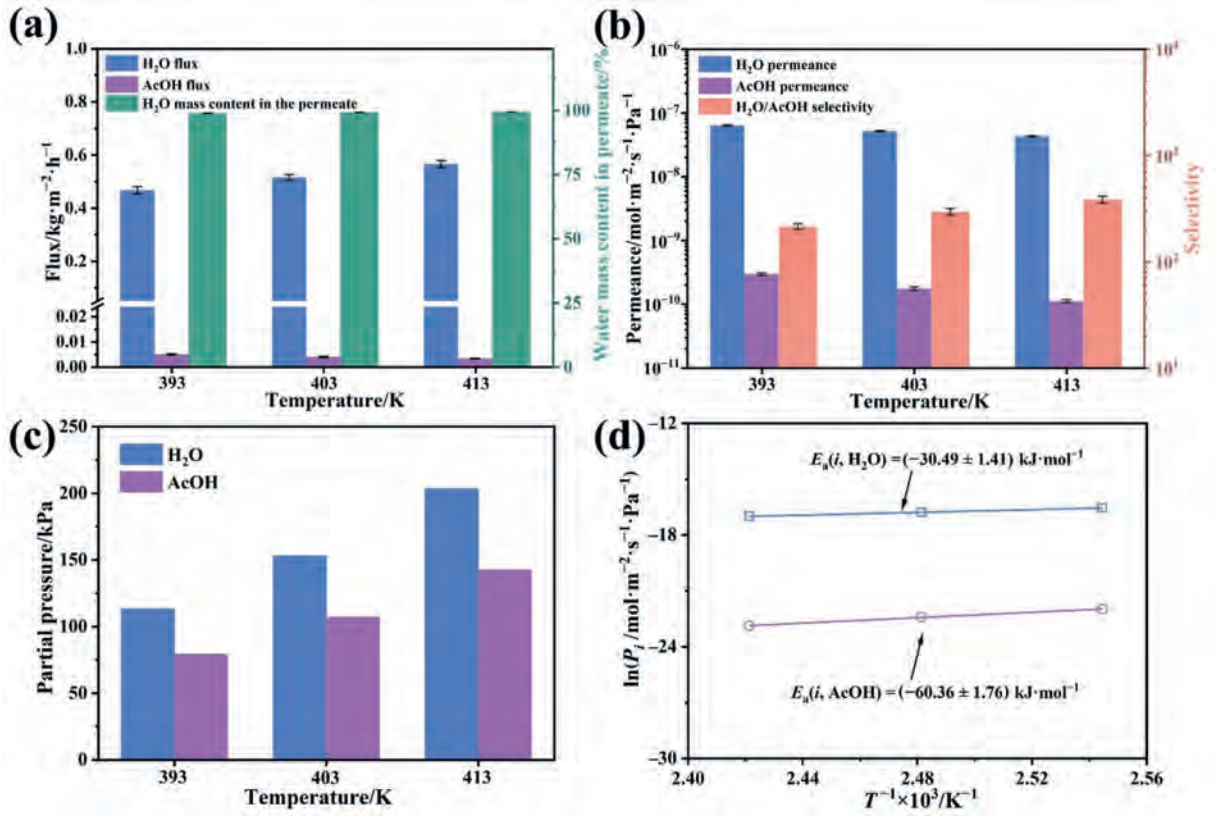

Fig. 6. (a) Flux and water mass content in the permeate, (b) permeance and selectivity, (c) partial pressure difference and (d) Arrhenius relationship of permeances as a function of temperature through the monolithic membrane M1 in a mass ratio of 30/70 water/AcOH mixture with a feed flow rate of 50 ml·min^{-1} (liquid base at standard state). An error bar is added.

were quantitively described through activation energy (E_a) analysis based on the Arrhenius relationship between permeance and temperature (Fig. 6(d)) [36]. The E_a values for water and AcOH were −30.49 ± 1.41 kJ·mol^{-1} and −60.36 ± 1.76 kJ·mol^{-1}, respectively. The negative value of E_a demonstrated that the separation was dominated by adsorption process. It was suggested that the decline in water and AcOH permeances within the temperature range of 393–413 K could be attributed to the reduced adsorption capacity of CHA zeolite membranes [37].

3.4. Effect of feed water content on VP for monolithic CHA zeolite membranes

Fig. 7 shows the effect of feed water content on the VP separation performance of water/AcOH mixtures through the monolithic membrane M1 at 393 K with a feed flow rate of 50 ml·min^{-1} (liquid base at standard state). As the water mass content in the feed increased from 5% to 30%, the water flux increased by 80%, and the water mass content in the permeate increased from 95% to 99% (Fig. 7(a)). Both water and AcOH permeances decreased as their partial pressures increased (Fig. 7(b)). It was the common trend for permeance since the increasing rate of loading/permeating amount (flux) was always lower than or sometimes equal to that of the concentration of the specie in the bulk mixture [38]. The partial pressure of water increased by nearly 6 times, while that of AcOH decreased by only 33% with the increase of feed water content (Fig. 7(c)). Flux is influenced not only by membrane characteristics but also by the driving force. As seen in Fig. 7, the increase in water flux was primarily attributed to the increase of the driving force. Most studies predominantly reported flux, while omitting the crucial parameter of permeance that reflects inherent separation capacity of the membrane, as validated by inverse correlations between water flux and permeance under different thermal/content conditions (Figs. 6 and 7). Therefore, it necessitated dual-parameter reporting (flux & permeance) for comprehensive evaluation of membrane performance.

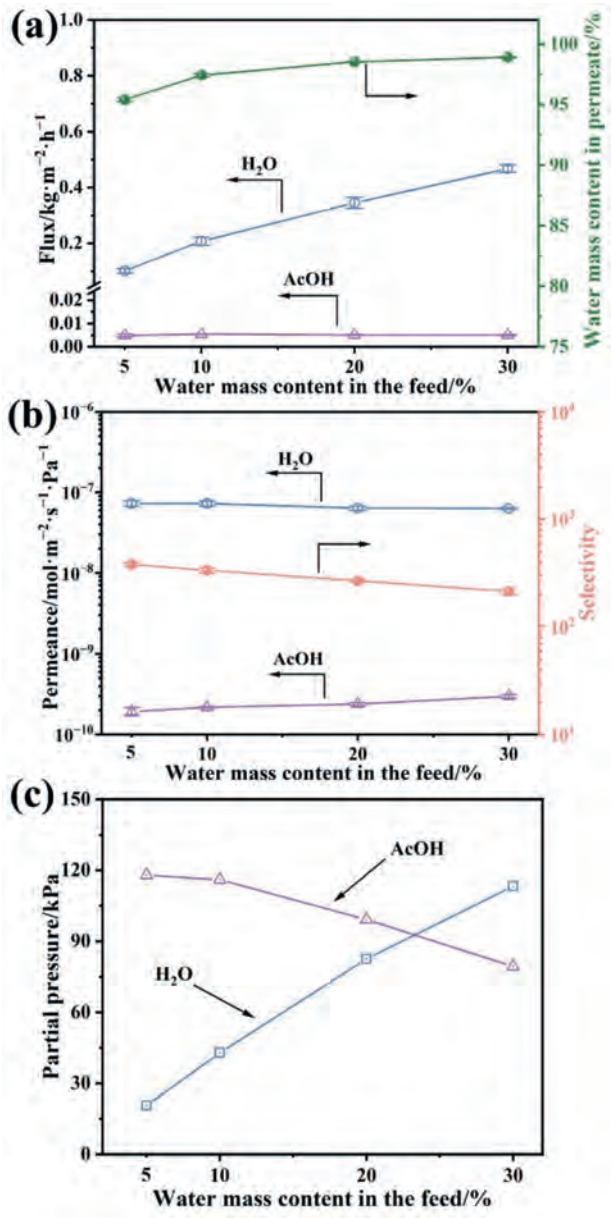

Fig. 7. (a) Flux and water mass content in the permeate, (b) permeance and selectivity and (c) partial pressure as a function of feed water content through the monolithic membrane M1 at 393 K with a feed flow rate of 50 ml·min^{-1} (liquid base at standard state). An error bar is added.

3.5. Effect of feed flow rate on VP for monolithic CHA zeolite membranes

Fig. 8 displays the effect of feed flow rate on the VP separation performance of the monolithic membrane M1 in the water/AcOH mixture. As the feed flow rate increased from 25 to 100 ml·min^{-1}, the water flux/permeance increased by 80% (from 0.35 to 0.63 kg·m^{-2}·h^{-1} and from 4.74 × 10^{-8} to 8.55 × 10^{-8} mol·m^{-2}·s^{-1}·Pa^{-1}, respectively), and the water/AcOH selectivity increased by 121% (from 167 to 369). As shown in Fig. 8 (c), the components of the partial pressures were independent of the feed flow rate. Concentration polarization (CP) critically limits membrane performance through interfacial accumulation of slow-permeating species (AcOH), as quantified by Reynolds number (*Re*). Herein, *Re* increased from 652 to 2610 with feed flow rate increasing from 25 to 100 ml·min^{-1} as shown in Fig. 8(c). Enhanced turbulence at higher *Re* effectively mitigated the negative effect of CP, concomitantly boosting water permeance and water/AcOH selectivity. These findings established flow regime engineering as a vital strategy for optimizing membrane separation efficiency [39]. It should be noted that the separation performance of current monolithic CHA zeolite membrane remained suboptimal due to the limitation of test flow rate of the laboratory-scale device.

3.6. Stability test of 19-channel monolithic CHA membrane in VP

To investigate the stability of the monolithic zeolite membrane, the continuous test was conducted for 48 h in a mass ratio of 30/70 water/AcOH mixture at 393 K, and a feed flow rate of 50 ml·min^{-1} as shown in Fig. 9. During the whole testing process, the water flux and permeance were stabilized at (0.41 ± 0.030) kg·m^{-2}·h^{-1} and (5.55 ± 0.45) × 10^{-8} mol·m^{-2}·s^{-1}·Pa^{-1}, respectively. Moreover, water mass content in the permeate was over 99% for 48 h testing. It demonstrates that the monolithic CHA zeolite membrane shows good stability under high-temperature and high-acidity conditions. The initial fluctuation of water flux could be attributed to the disequilibrium state of adsorption and desorption of water molecules on CHA zeolite [40].

3.7. Characterization of 19-channel monolithic CHA membrane after VP test

Fig. 10 shows typical SEM images of the surface and cross-section views of the monolithic membrane M1 after VP testing.

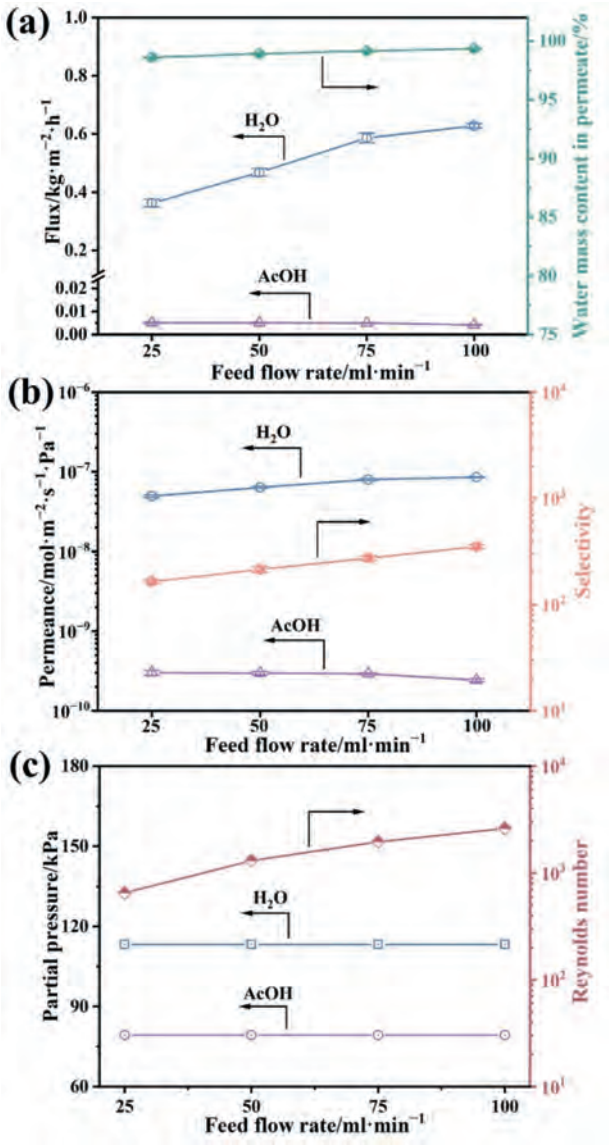

Fig. 8. (a) Flux and water mass content in the permeate, (b) permeance and selectivity and (c) partial pressure and Reynolds number as a function of feed flow rate (liquid base at standard state) through the monolithic membrane M1 in a mass ratio of 30/70 water/AcOH mixture at 393 K. An error bar is added.

The surface images (Fig. 10(a)–(c)) displayed the intergrown zeolite layers formed on the exterior, middle and interior channels of the monolithic membrane had similar morphologies to the fresh ones; no detectable defects (pinholes/cracks) were observed. Cross-sectional observation of monolithic membrane (Fig. 10(d)–(f)) confirmed that membrane integrity was preserved. The XRD characteristic diffraction peaks of zeolite membranes after VP testing (Fig. 11) at typical positions were similar to the fresh ones as shown in Fig. 4. These observations from SEM and XRD characterization in Figs. 10 and 11 together with the stability testing in Fig. 9 conclusively established that the membrane was stable in the acidic medium [40].

3.8. Comparison with the literatures

Table 1 lists the separation performance of the current large-area monolithic CHA zeolite membrane with that of other small-

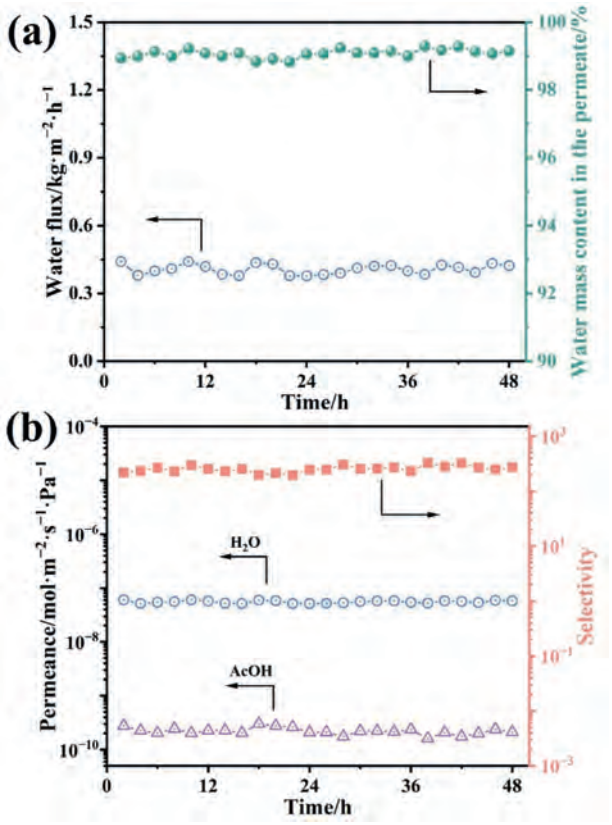

Fig. 9. (a) Flux and water mass content in the permeate, (b) permeance and selectivity as a function of test time through the monolithic membrane M1 at 393 K in a 70% (mass) AcOH aqueous solution with a feed flow rate of 50 ml·min^{-1} (liquid base at standard state).

area zeolite membranes for separation of water/AcOH mixtures. Nagase *et al.* [41] demonstrated a MER zeolite membrane (15.7 cm^2) on mullite tubular supports achieving a water flux of 0.1 kg·m^{-2}·h^{-1} with exceptional selectivity of 8991 by PV at 313 K for dehydration of 90% (mass) AcOH aqueous solution. Xu *et al.* [42] prepared LTA@GO composite membranes (2.5 cm^2) on porous alumina discs to improve the acid stability of LTA membranes and exhibited better dehydration performance in a 95% (mass) AcOH solution at 333 K (water flux of 1.5 kg·m^{-2}·h^{-1}, separation factor of 400), but the long-term stability was not detected. Zhang *et al.* [37] successfully fabricated high-quality DD3R zeolite membranes (4 cm^2) on the outside surface of ceramic hollow fiber support. They demonstrated excellent water-selective permeation with a water flux of 0.58 kg·m^{-2}·h^{-1} and a separation factor of 800 in the dehydration of a mass ratio of 30/70 water/AcOH mixture at 368 K. Si *et al.* [43] prepared high-alumina ZSM-5 zeolite membranes (37.7 cm^2) on tubular mullite supports using a fluorine-containing and organic template-free synthesis gel. The membranes demonstrated good separation performance, maintaining a water flux of 0.72 kg·m^{-2}·h^{-1} and a separation factor of >3000.

The previous fabrication of zeolite membranes predominantly employed tubular, hollow fiber, and disk-shaped supports. These conventional geometries of membranes imposed fundamental limitations for industrial-scale implementation including low packing density for the module and/or poor mechanical strength. Herein, 19-channel monolithic CHA zeolite membranes had advantages such as large membrane area, high mechanical strength and high packing density. The large-area monolithic membrane

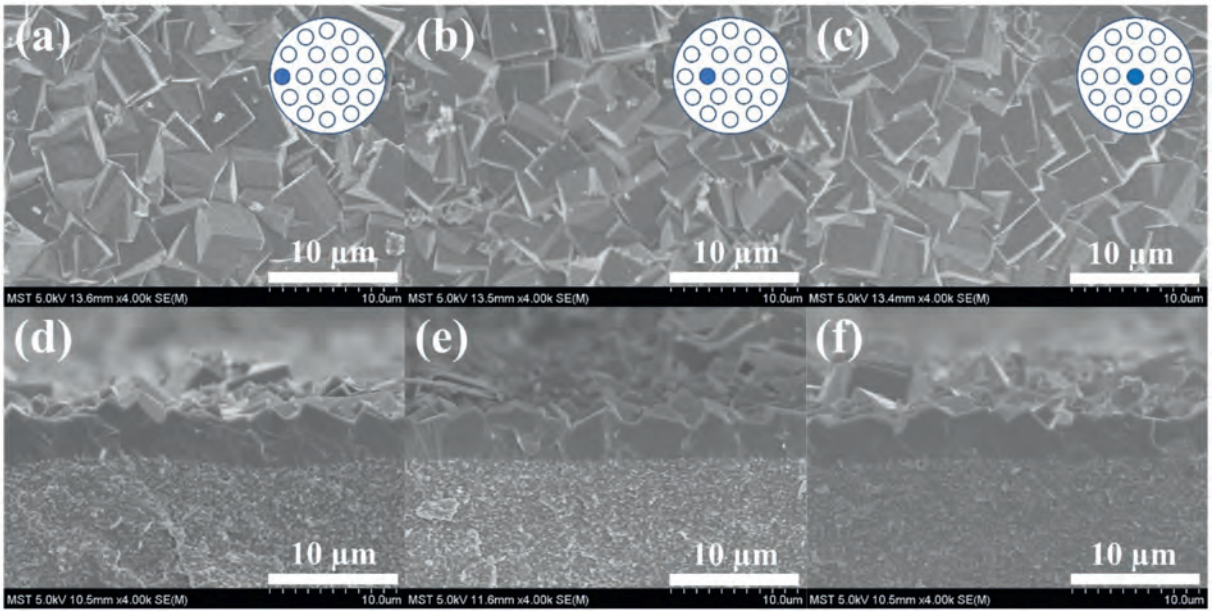

Fig. 10. SEM images of the surface and cross-section of zeolite membranes on the (a, d) exterior, (b, e) middle and (c, f) interior channels of the monolithic membrane M1 after VP testing.

Table 1
Comparison of separation performance of the 19-channel monolithic CHA zeolite membrane prepared in this study with other reported zeolite membranes for separation of water/AcOH mixtures.

Membrane type	Membrane area/cm^2	Support dimension	Water/AcOH mixture/% (mass)	Temperature/K	Water flux/$kg \cdot m^{-2} \cdot h^{-1}$	Separation factor (selectivity)	Ref.
MER	15.7	Porous mullite tube	10/90	313	0.1	8991	[41]
ZSM-5	37.7	Porous mullite tube	50/50	348	2.21	200	[44]
ZSM-5	37.7	Porous mullite tube	10/90	348	0.71	3200	[43]
UZM-5	2.5	Porous α-Al_2O_3 disk	10/90	338	0.8	989	[45]
LTA@GO	2.5	Porous α-Al_2O_3 disk	5/95	333	1.5	400	[42]
CHA	30	Porous α-Al_2O_3 tube	30/70	348	2.1	401	[23]
CHA	5.8	Outside, 4-channel α-Al_2O_3 hollow fiber	50/50	348	2.5	49	[22]
DD3R	4	Outside, 4-channel α-Al_2O_3 hollow fiber	70/30	368	0.58	800	[37]
CHA	140	Inside, 19-channel α-Al_2O_3 monolith	30/70	393	0.63	369 (369)	This work

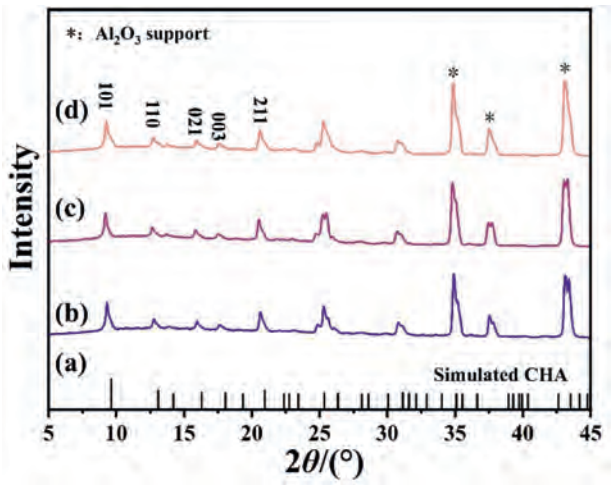

Fig. 11. XRD patterns of (a) simulated CHA framework and zeolite membranes on the typical (b) exterior, (c) middle and (d) interior channels of the monolithic membrane M1 after VP testing.

displayed a water flux of 0.63 $kg \cdot m^{-2} \cdot h^{-1}$ and selectivity of 369 at 393 K in a mass ratio of 30/70 water/AcOH mixture. Such separation performance was comparable to these of reported small-area zeolite membranes as shown in Table 1. Please note that the current test results were subjected to the limit of feed flow rate of the test setup. Separation performance of this monolithic membrane should be further improved if the feed flow rate increases further. On the other hand, water permeance could increase once the resistance of mass transfer reduces. In our future work, we will modify membrane synthesis to reduce membrane thickness, and the overgrowth of crystals in support pores to further increase the water permeance of the monolithic membranes. It demonstrates that the 19-channel monolithic CHA zeolite membrane is a promising candidate for addressing the crucial limitation in the dehydration of AcOH.

4. Conclusions

Large-area CHA zeolite membranes were successfully prepared from high-silica gel with SiO_2/Al_2O_3 ratio of 200 on 19-channel α-Al_2O_3 monolithic supports and were used for VP separation of water/AcOH mixtures for the first time. The membranes grown on

each channel exhibited a uniform thickness of 4.2–4.5 μm and similar intergrown crystal morphology. Ideal H_2/SF_6 selectivities of three monolithic CHA zeolite membranes were higher than 185, indicating that the membranes have high quality and membrane synthesis is reproducible. The improvement of temperature and feed water content in VP testing is beneficial to enhance water flux, while permeance present the opposite trend. CP emerges as the primary performance-limiting factor for the large-area monolithic membrane reduced both water permeance and water/AcOH selectivity. Increasing feed flow rate could reduce the negative influence of CP. Limited by the current test feed flow rate, the current monolithic CHA zeolite membrane displayed a water flux, water permeance and water/AcOH selectivity of 0.63 $kg \cdot m^{-2} \cdot h^{-1}$, 8.56×10^{-8} $mol \cdot m^{-2} \cdot s^{-1} \cdot Pa^{-1}$ and 369 at 393 K in a mass ratio of 30/70 water/AcOH mixture. Such separation performance was comparable to that of the reported small-area ones. The membrane displayed good stability under harsh VP test conditions. This work pioneers the implementation of monolithic CHA zeolite membranes in dehydration of AcOH *via* VP due to their high surface-to-volume ratio, large area, good separation performance and high stability.

CRediT Authorship Contribution Statement

Hong Xiao: Writing – review & editing, Methodology, Writing – original draft, Investigation. Shilei Yu: Formal analysis, Writing – review & editing, Data curation. Yuhan Yan: Formal analysis, Writing – review & editing, Data curation. Junjing Zhou: Funding acquisition, Writing – review & editing. Rongfei Zhou: Supervision, Conceptualization, Writing – review & editing, Funding acquisition. Weihong Xing: Writing – review & editing, Funding acquisition, Supervision.

Data Availability

No data was used for the research described in the article.

Declaration of Competing Interest

The authors declare that they have no known competing financial interests or personal relationships that could have appeared to influence the work reported in this paper.

Acknowledgements

This work was financially supported by the National Key Research and Development Program of China (2023YFB3810700), the National Natural Science Foundation of China (22378189, U22A20414 and 22378188), the Natural Science Foundation of Jiangsu Provincial Department of Science and Technology (BK20232010 and BG2024018), and National State Key Laboratory of Material-oriented Chemical Engineering (SKL-MCE-22A02 and SKL-MCE23B14).

References

[1] G. Merli, A. Becci, A. Amato, F. Beolchini, Acetic acid bioproduction: The technological innovation change, *Sci. Total Environ.* 798 (2021) 149292.
[2] I.M. Pérez-Díaz, R.F. McFeeters, Microbiological preservation of cucumbers for bulk storage using acetic acid and food preservatives, *J. Food Sci.* 73 (2008) M287–M291.
[3] J.L. Martín-Espejo, J. Gandara-Loe, J.A. Odriozola, T.R. Reina, L. Pastor-Pérez, Sustainable routes for acetic acid production: Traditional processes vs a low-carbon, biogas-based strategy, *Sci. Total Environ.* 840 (2022) 156663.
[4] G.J. Sunley, D.J. Watson, High productivity methanol carbonylation catalysis using iridium The Cativa™ process for the manufacture of acetic acid, *Catal. Today* 58 (4) (2000) 293–307.
[5] T. Tsuru, T. Shibata, J.H. Wang, H.R. Lee, M. Kanezashi, T. Yoshioka, Pervaporation of acetic acid aqueous solutions by organosilica membranes, *J. Membr. Sci.* 421 (2012) 25–31.
[6] N. Jullok, P. Luis, J. Degrève, B. van der Bruggen, A cascaded pervaporation process for dehydration of acetic acid, *Chem. Eng. Sci.* 105 (2014) 208–212.
[7] G.P. Liu, W.Q. Jin, Pervaporation membrane materials: Recent trends and perspectives, *J. Membr. Sci.* 636 (2021) 119557.
[8] L.Q. Li, J.J. Li, L.J. Cheng, J.X. Wang, J.H. Yang, Microwave synthesis of high-quality mordenite membrane by a two-stage varying heating-rate procedure, *J. Membr. Sci.* 612 (2020) 118479.
[9] F.Z. Charik, B. Achiou, A. Belgada, Z.C. Elidrissi, M. Ouammou, M. Rabiller-Baudry, S.A. Younssi, Optimal preparation of low-cost and high-permeation NaA zeolite membrane for effective ethanol dehydration, *Microporous Mesoporous Mater.* 344 (2022) 112229.
[10] K.I. Okamoto, H. Kita, K. Horii, K.T. Kondo, Zeolite NaA membrane: preparation, single-gas permeation, and pervaporation and vapor permeation of water/organic liquid mixtures, *Ind. Eng. Chem. Res.* 40 (1) (2001) 163–175.
[11] H. Kita, K. Horii, Y. Ohtoshi, K. Tanaka, K.I. Okamoto, Synthesis of a zeolite NaA membrane for pervaporation of water/organic liquid mixtures, *J. Mater. Sci. Lett.* 14 (3) (1995) 206–208.
[12] L.Z. Li, Y. Lu, L.Q. Li, J.H. Yang, W.J. Fu, Y.W. Luo, J.M. Lu, Y. Zhang, L. Zhou, Highly selective zeolite T membranes with different ERI stacking faults for pervaporative dehydration of ethanol, *J. Membr. Sci.* 638 (2021) 119701.
[13] J. Kuhn, K. Yajima, T. Tomita, J. Gross, F. Kapteijn, Dehydration performance of a hydrophobic DD3R zeolite membrane, *J. Membr. Sci.* 321 (2) (2008) 344–349.
[14] X. Lin, E. Kikuchi, M. Matsukata, Preparation of mordenite membranes on α-alumina tubular supports for pervaporation of water–isopropyl alcohol mixtures, *Chem. Commun. (11) (2000) 957–958.*
[15] Q. Wang, C. Qian, C.X. Guo, N. Xu, Q. Liu, B. Wang, L. Fan, K.H. Hu, Pervaporation dehydration mechanism and performance of high-aluminum ZSM-5 zeolite membranes for organic solvents, *Int. J. Mol. Sci.* 25 (14) (2024) 7723.
[16] X. Lin, H. Kita, K.I. Okamoto, Silicalite membrane preparation, characterization, and separation performance, *Ind. Eng. Chem. Res.* 40 (19) (2001) 4069–4078.
[17] Q. Liu, R.D. Noble, J.L. Falconer, H.H. Funke, Organics/water separation by pervaporation with a zeolite membrane, *J. Membr. Sci.* 117 (1–2) (1996) 163–174.
[18] T. Sano, H. Yanagishita, Y. Kiyozumi, F. Mizukami, K. Haraya, Separation of ethanol/water mixture by silicalite membrane on pervaporation, *J. Membr. Sci.* 95 (3) (1994) 221–228.
[19] Y. Cui, H. Kita, K.I. Okamoto, Zeolite T membrane: preparation, characterization, pervaporation of water/organic liquid mixtures and acid stability, *J. Membr. Sci.* 236 (1–2) (2004) 17–27.
[20] J. Jiang, L. Peng, X.R. Wang, H. Qiu, M.M. Ji, X.H. Gu, Effect of Si/Al ratio in the framework on the pervaporation properties of hollow fiber CHA zeolite membranes, *Microporous Mesoporous Mater.* 273 (2019) 196–202.
[21] Y. Hasegawa, H. Hotta, K. Sato, T. Nagase, F. Mizukami, Preparation of novel chabazite (CHA)-type zeolite layer on porous α-Al_2O_3 tube using template-free solution, *J. Membr. Sci.* 347 (1–2) (2010) 193–196.
[22] H. Qiu, J. Jiang, L. Peng, H. Liu, X.H. Gu, Choline chloride templated CHA zeolite membranes for solvents dehydration with improved acid stability, *Microporous Mesoporous Mater.* 284 (2019) 170–176.
[23] S. Imasaka, M. Itakura, K. Yano, S. Fujita, M. Okada, Y. Hasegawa, C. Abe, S. Araki, H. Yamamoto, Rapid preparation of high-silica CHA-type zeolite membranes and their separation properties, *Sep. Purif. Technol.* 199 (2018) 298–303.
[24] H.L. Hong, K.L. Yu, H.B. Liu, R.F. Zhou, W.H. Xing, Industrial-scale 61-channel monolithic silicalite-1 membranes for butane isomer separation, *Adv. Membr.* 4 (2024) 100096.
[25] Z.G. Xue, Y. Shen, L. Chen, B. Liu, N. Hu, R.F. Zhou, W.H. Xing, High-performance 19-channel monolithic chabazite membranes for efficient separation of water/ethanol and water/isopropanol mixtures by pervaporation and vapor permeation, *J. Membr. Sci.* 713 (2025) 123353.
[26] B. Liu, R. Zhang, Y. Du, F. Gao, J.J. Zhou, R.F. Zhou, Highly selective high-silica SSZ-13 zeolite membranes for H_2 production from syngas, *Int. J. Hydrogen Energy* 45 (32) (2020) 16210–16218.
[27] L. Yu, M.S. Nobandegani, A. Holmgren, J. Hedlund, Highly permeable and selective tubular zeolite CHA membranes, *J. Membr. Sci.* 588 (2019) 117224.
[28] D. Korelskiy, T. Leppäjärvi, H. Zhou, M. Grahn, J. Tanskanen, J. Hedlund, High flux MFI membranes for pervaporation, *J. Membr. Sci.* 427 (2013) 381–389.
[29] M. Pera-Titus, J. Llorens, F. Cunill, R. Mallada, J. Santamaría, Preparation of zeolite NaA membranes on the inner side of tubular supports by means of a controlled seeding technique, *Catal. Today* 104 (2–4) (2005) 281–287.
[30] X.Q. Mo, H.B. Liu, Y.L. Li, Q.L. Gu, B. Wang, R.F. Zhou, W.H. Xing, SSZ-13 membranes on novel silica carbide monoliths for efficient CO_2 separation, *J. Membr. Sci.* 699 (2024) 122642.
[31] J.J. Zhou, S.J. Wu, B. Liu, R.F. Zhou, W.H. Xing, Scalable fabrication of highly selective SSZ-13 membranes on 19-channel monolithic supports for efficient CO_2 capture, *Sep. Purif. Technol.* 293 (2022) 121122.
[32] Y.M. Li, Y.L. Wang, M.Y. Guo, B. Liu, R.F. Zhou, Z.P. Lai, High-performance 7-channel monolith supported SSZ-13 membranes for high-pressure CO_2/CH_4 separations, *J. Membr. Sci.* 629 (2021) 119277.
[33] S. Kobuchi, K. Takakura, S. Yonezawa, K. Fukuchi, Y. Arai, Correlation of vapor–liquid equilibria of binary systems containing carboxylic acid by using Wilson equation with parameters estimated from pure-component properties, *J. Chem. Eng. Jpn.* 46 (2) (2013) 100–106.

[34] D.H. Olson, M.A. Camblor, L.A. Villaescusa, G.H. Kuehl, Light hydrocarbon sorption properties of pure silica Si-CHA and ITQ-3 and high silica ZSM-58, *Microporous Mesoporous Mater.* 67 (1) (2004) 27–33.
[35] N.N. Wang, N. Liu, J.J. Zhou, Q. Wang, N. Hu, R.F. Zhou, Large-area, high-permeance and acid-resistant zeolite SSZ-13 membranes for efficient pervaporative separation of water/acetic acid mixtures, *J. Membr. Sci.* 691 (2024) 122251.
[36] Y.T. Zhang, X.F. Zhu, S.Z. Chen, J.Y. Liu, Z. Hong, J.C. Wang, Z. Li, X.C. Gao, R. Xu, X.H. Gu, TiO_2-decorated NaA zeolite membranes with improved separation stability for pervaporation dehydration of N, N-Dimethylacetamide, *J. Membr. Sci.* 634 (2021) 119398.
[37] Y.T. Zhang, S.Z. Chen, R. Shi, P. Du, X.F. Qiu, X.H. Gu, Pervaporation dehydration of acetic acid through hollow fiber supported DD3R zeolite membrane, *Sep. Purif. Technol.* 204 (2018) 234–242.
[38] R.W. Baker, J.G. Wijmans, Y. Huang, Permeability, permeance and selectivity: a preferred way of reporting pervaporation performance data, *J. Membr. Sci.* 348 (1–2) (2010) 346–352.
[39] J.H. Chen, J.Z. Zheng, Q.L. Liu, H.X. Guo, W. Weng, S.X. Li, Pervaporation dehydration of acetic acid using polyelectrolytes complex (PEC)/11-phosphotungstic acid hydrate (PW11) hybrid membrane (PEC/PW11), *J. Membr. Sci.* 429 (2013) 206–213.
[40] Y.Q. Li, M.H. Zhu, N. Hu, F. Zhang, T. Wu, X.S. Chen, H. Kita, Scale-up of high performance mordenite membranes for dehydration of water-acetic acid mixtures, *J. Membr. Sci.* 564 (2018) 174–183.
[41] T. Nagase, Y. Kiyozumi, Y. Hasegawa, T. Inoue, T. Ikeda, F. Mizukami, Dehydration of concentrated acetic acid solutions by pervaporation using novel MER zeolite membranes, *Chem. Lett.* 36 (5) (2007) 594–595.
[42] K. Xu, Z.Q. Jiang, B. Feng, A.S. Huang, A graphene oxide layer as an acid-resisting barrier deposited on a zeolite LTA membrane for dehydration of acetic acid, *RSC Adv.* 6 (28) (2016) 23354–23359.
[43] D.Y. Si, M.H. Zhu, X.M. Sun, M. Xue, Y.Q. Li, T. Wu, T. Gui, I. Kumakiri, X.S. Chen, H. Kita, Formation process and pervaporation of high aluminum ZSM-5 zeolite membrane with fluoride-containing and organic template-free gel, *Sep. Purif. Technol.* 257 (2021) 117963.
[44] M.H. Zhu, I. Kumakiri, K. Tanaka, H. Kita, Dehydration of acetic acid and esterification product by acid-stable ZSM-5 membrane, *Microporous Mesoporous Mater.* 181 (2013) 47–53.
[45] R. Yao, Y. Peng, H.L. Song, C.Y. Zhu, P.Y. Wang, L. Kun, W.S. Yang, Rational design and fabrication of a novel acid-resistant UZM-5 zeolite membrane for pervaporation dehydration processes, *Chem. Commun.* 57 (75) (2021) 9574–9577.